ORIGINAL CONTRIBUTION

Homogeneous nucleation in polyamide 66, a two-stage process as revealed by combined nanocalorimetry and IR spectroscopy

Wycliffe Kiprop Kipnusu[1] · Evgeny Zhuravlev[2] · Christoph Schick[3] · Friedrich Kremer[1]

Abstract

Nanocalorimetry and Fourier transform infrared (FTIR) spectroscopy are combined to measure the calorimetric properties and molecular spectra of the same sample (sample amount about 5 ng) of polyamide 66 (PA66). By determining IR difference absorption spectra between a quenched and a sample annealed at varying temperatures (T_a) and annealing time (t_a), the initial steps of homogeneous nucleation is for the first time revealed on a molecular scale, long before crystallization takes place. As starting point (i), isolated H-bonds are formed between (N–H) and (C=O) moieties of adjacent (neighboring) polymer segments promoted by far-reaching dipole–dipole interactions. In the second step (ii), the H-bonds realign, which in part requires the opening of already established H-bonds. In stage (i), the FTIR absorption intensity of the free $(C=O)_f$ moieties decreases while that of the H-bonded $(C=O)_b$ ones increases as a function of T_a at constant t_a. This implies an increase in the H-bonding network in amorphous domains. The second stage of nucleation in the studied PA66 is characterized by an increase in the number of $(C=O)_f$ and a corresponding decrease in $(C=O)_b$ moieties as the sample transitions to the ordered crystalline structure. This is attributed to a change from γ to α polymorphs in PA66. The non-polar methylene units in PA66 are largely unaffected during the nucleation steps, where no changes in the overall heat capacity are detectable, proving that these changes occur prior to the onset of crystal growth.

Keywords Nucleation · Polyamide · Calorimetry · Infrared · Polymorph · Crystallization

Introduction

The crystal nucleation is considered as a nascent stage that controls crystal structure/polymorphs in many crystalline materials. Different crystal polymorphs with distinct macroscopic properties are therefore traced back to the nucleation mechanisms which is easily affected by the material's processing conditions [1, 2]. Understanding the mechanism of homogeneous nucleation (HN) that take place before crystallisation is not only important for industrial processes but it is also a valid fundamental scientific quest. Molecular

mechanism during the initial stages of HN is largely unexplored because of a lack of suitable experimental techniques to observe the process in real time. Recently, we developed a technique that combines fast scanning calorimetry (FSC) also known as nanocalorimetry and Fourier transform infrared (FTIR) spectroscopy to monitor the nucleation at the molecular level [3]. This method is employed in the current study to trace more details in the nucleation process in a polyamide 66 (PA66) sample.

In contrast to the heterogeneous nucleation which take place in the presence of external interfaces such as sample substrates or small foreign particles in the sample, the HN takes place due to self-organization of the molecular units within the bulk sample [4]. One of the methods to access the HN process is by reducing the sample size to nanoscale and then rapidly quenching (at cooling rate in the order 10^3–10^6 K/s) from its molten state to temperatures where isothermal annealing is carried out [5]. This is made possible by the use of the nanocalorimetry technique which helps to avoid crystallisation during cooling [6] and hence transform the sample into a pure amorphous state. This is also

✉ Wycliffe Kiprop Kipnusu
kipnusu@physik.uni-leipzig.de

1   Peter Debye Institute for Soft Matter Physics, Leipzig University, Linnestr. 5, 04103 Leipzig, Germany

2   Institute of Physics and Competence Centre, University of Rostock, Albert-Einstein-Str. 23-24, 18059 Rostock, Germany

3   Institute of Chemistry, Kazan Federal University, Kazan 42000008, Russian Federation

possible at lower cooling rate when the sample is reduced to nanoscale [7]. Nucleation is then monitored under iso-thermal conditions. In this respect, nanocalorimetry is used to first pre-condition the sample and to analyse kinetic and thermodynamic phase transformations. Structural trans-formations on the same non-equilibrium conditions of the sample can be obtained by combining information from nanocalorimetry with data from other methods [8] such as polarized optical microscopy [9–11], X-ray diffraction [9], atomic force microscopy [12], Raman spectroscopy [13], and FTIR spectroscopy [3]. The importance of the latter two techniques is that they enable in situ monitoring of the nucleation process from the molecular level in combination with the information on the phase transformation from nano-calorimetry. However, Raman spectroscopy has a drawback that laser heating can induce unintended temperature change in the sample [13]. On the other hand, FTIR being non-destructive allows for repeated measurement and hence is able to follow local conformation and interaction between polymer segments. Indeed, FTIR spectroscopy has been used extensively as a highly efficient tool in monitoring hydrogen bond induced changes in different polyamides [14–20].

H-bond bridges play a critical role in the nucleation and crystallization processes in PA samples. Li et al. [21] found that high H-bond density favours fast crystallization due to thermodynamic driving forces at higher temperatures. In most cases, H-bond causes a red-shift of the IR frequency position and an increase in the level of IR absorption [22–24]. A change in H-bond length is also related to the structural changes in the sample. Information about H-bond length and density in PA66 in the amorphous state is lack-ing. Only in the low molecular weight systems, e.g. poly-alcohol, the relationship between the stretching vibrations ν(OH), the separation distance of the OH—O bonds, and the density is known in a wide temperature range [25]. In poly-amides, nearly all the amide units that separate a sequence of methylene groups are H-bonded [26, 27] and their density determine the respective melting temperatures of aliphatic homopolyamides [28]. For PA6, Zhang et al. found that the changes in amide and methylene bands provide evidence of three crystalline modifications in PA6 from melt crystalliza-tion associated with different polymorphs [20].

Despite extensive studies of different polymorphs in poly-amide polymers, controversies still exist [29–32]. X-ray stud-ies have identified two polymorphs, namely γ and α phases in PA6 samples [29] but also in even-even polyamides such as PA66 [9, 30]. Pseudo-hexagonal mesophases referred to as β phase also exist at lower temperatures. Similarly, studies by nanocalorimetry reveal two distinct crystallization rate maxima that is attributed to the formation of different crys-tal polymorphs or changes in the mechanism of nucleation growth [5]. Intuitively, the different polymorphs observed in the crystalline state samples should have their origin from

different nucleation pathways [33]. Nucleation determines whether a phase will form, how the formation will occur and what structure will be formed [34–36]. It is a dynamic process that is controlled by the interplay between reduced bulk free energy and increased surface energy and begins with metastable structures which undergo transition to stable structures depending on the critical size of the nuclei [34]. Nucleation mechanism is discussed in the framework of the classical and non-classical nucleation theories. According to the classical nucleation theory, nucleation is thought to undergo a single step in which the clusters that attain the critical size continue to grow spontaneously while in non-classical nucleation theory, more steps are introduced to describe the intermediate states as observed in experiments [37, 38]. Several computer simulations and experiments point to the existence of a two-step nucleation mechanism in complex molecules like proteins and synthetic polymers [39–41].

In this paper, we investigate the onset and progress of homogeneous nucleation in PA66 at the molecular level by performing in situ nanocalorimetry and FTIR spectroscopy. This was achieved by using a modified calorimetric chip sensor that also enables FTIR spectroscopic characterisation on the same sample. Owing to this arrangement, we were able to heat and cool the sample at an ultrahigh rate to the desired temperatures and hence obtain the pure amorphous state of the sample before monitoring the nucleation process as function of annealing temperature and time. We observed a two-stage process during nucleation. This is attributed to the formation of higher density regions within the amor-phous phase, where metastable structures develop and then transform to the more stable crystalline phase.

Materials and methods

Polyamide 66 (PA66) film of thickness 0.017 mm was pur-chased from Goodfellow GmbH and used as received. In order to allow for combined FSC and FTIR measurements on the same sample, PA66 (about 5–10 ng) was prepared directly on the calorimetric sensor (Fig. 1a) having a trans-parent silicon nitride (SiN) membrane. Details of the sample preparation are described in Ref. [3]. Briefly, the sample was cut under a microscope into a small piece of about 100 μm in diameter. This piece was then placed onto the FSC chip sen-sor and transferred to a sample preparation heating stage in a gas purged box. The box was continuously flushed with dry nitrogen to avoid sample water absorption and degrada-tion on heating. The temperature was then increased slowly until the PA66 sample started to melt. While still in nitrogen atmosphere, the molten state of PA66 was gently spread on the sensor using a thin platinum wire in order to achieve suitable sample thickness for the FTIR measurement. Excess
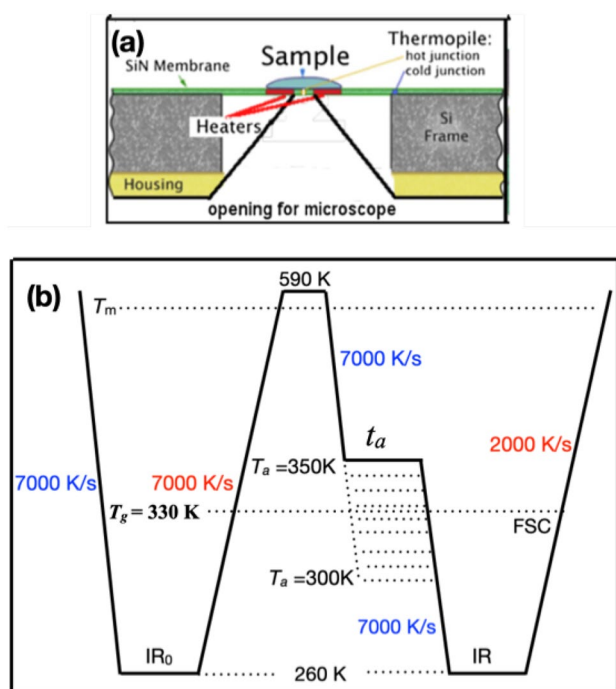
Fig. 1 **a** Scheme of the sample geometry for the combined FSC and FTIR spectroscopy. The sample (about 5 ng) is placed on an IR transparent silicon nitride (SiN) membrane that is in contact with resistive heaters. **b** Temperature profile employed for the combined FSC and FTIR measurements after subsequent annealing steps at different temperatures (T_a) and constant annealing times (t_a)

material was removed in the process. The whole process was done under the microscope.

An FSC device (designed in the University of Rostock, Germany) was employed for thermal pre-conditioning of the sample and for obtaining the FSC scans for analysis. In FSC, opto-sensor XEN 39,469 from Xensor Integration was used. The calorimeter chip with the sample was placed in a modified Linkam stage at 251 K in nitrogen atmosphere. IR measurements were carried out using a BioRad FTS 6000 FTIR spectrometer equipped with a UMA500 IR microscope and a mercury-cadmium-telluride (MCT) detector (Kolmar Technologies, Inc., USA) at a resolution of 2 cm^{-1}. FTIR measurements were recorded between 5000 and 1000 cm^{-1} in the transmission mode through a spot of diameter 100 μm. A single spectrum was obtained after averaging 128 scans collected within 80 s. The sample was first melted at 590 K for 0.1 s and then rapidly quenched to 260 K at 7000 K/s to obtain the fully amorphous sate. First IR measurements were recorded at this vitrified state and labelled IR$_0$. To erase thermal history, the sample was again melted at 590 K for 0.1 s and quenched at 7000 K/s to a specific annealing temperature (T_a) where it was held for a specific time (t_a) and then finally quenched further to 260 K. FTIR measurement (IR) and subsequent FSC scans at 2000 K/s were then carried out

and repeated for different T_a and t_a. The above procedure is summarised in Fig. 1b.

Results and discussion

The combined FSC and FTIR results of the identical PA66 sample are depicted in Fig. 2. The measured FSC signals represented by the apparent heat capacity as function of temperatures (Fig. 2a, b) show exothermic peaks due to the nucleation process also known as cold crystallization between 400 and 450 K. The area of these peaks is proportional to the number and /or size of the nuclei formed under isothermal annealing. The peak area finally decreases if nuclei already grow to crystals during the isotherm. Pure nucleation without the presence of crystal growth is confirmed when the integrated area of nucleation peak is equal to that of the melting peak. The FSC signal for T_a ranging from 300 to 450 K at $t_a = 10$ s (Fig. 2a) imply that nucleation primarily takes place at $T_a < 330$ K before crystal growth dominates for higher T_a. Under the cooling rates employed in this study, the T_g of PA66 is about 330 K hence the above observation is in accord with the finding that homogeneous nucleation is more effective at temperatures slightly below T_g [12]. When T_a is kept at 320 K and t_a varied between 1 and 10 s, PA66 remains within the nucleation regime as shown in Fig. 2b. More details of these processes are discussed later with consideration of how respective enthalpies change with T_a.

Similar observations discussed above can also be inferred from FTIR data presented in Fig. 2c, d. FTIR presents vital additional information about the changes occurring to the sample at the molecular level. The dominant IR absorption peaks at around 3300, 1650, and 1550 cm^{-1} represent stretching vibrations of ν(N–H), ν(C=O) (amide I) and combination of bending and stretching vibrations of δ(N–H) and ν(C-N) (amide II), respectively. It is important to note that the changes in the IR spectra during the nucleation process are very subtle hence it is more informative to present the data in the form of the difference spectra. An example of this analysis is shown in Fig. 3 for the amide I and II regions of the IR spectra. The original IR spectrum for $T_a = 315$ K and $t_a = 5$ s is shown in Fig. 3a. The red line is a fit to the data by a combination of Gaussian functions whose convolutions are represented by coloured regions. The amide I band show three contributions assigned to free ν(C=O)$_b$ moieties at around 1672 cm^{-1} and two H-bonded ν(C=O)$_b$ groups at around 1640 and 1620 cm^{-1} [18, 42]. An amide II band is characterized by the main peak at 1563 cm^{-1} and weaker contributions at 1560 cm^{-1} and 1517 cm^{-1}. Amide I and II bands together with ν(N–H) vibrations are more sensitive to structural changes taking place in the PA66 sample owing to their propensity to form the H-bond network.

More details of the evolution of the FTIR spectra (in form of difference spectra) due to the H-bond network during isothermal annealing at $t_a = 5$ s and the selected T_a are shown

Fig. 2 Fast scanning calorimetry scans of PA66 at heating rate 2000 K/s for **a** selected annealing temperatures T_a at an annealing time $t_a = 10$ s and **b** varying t_a at $T_a = 320$ K. The corresponding FTIR spectra are depicted in **c** and **d**, respectively
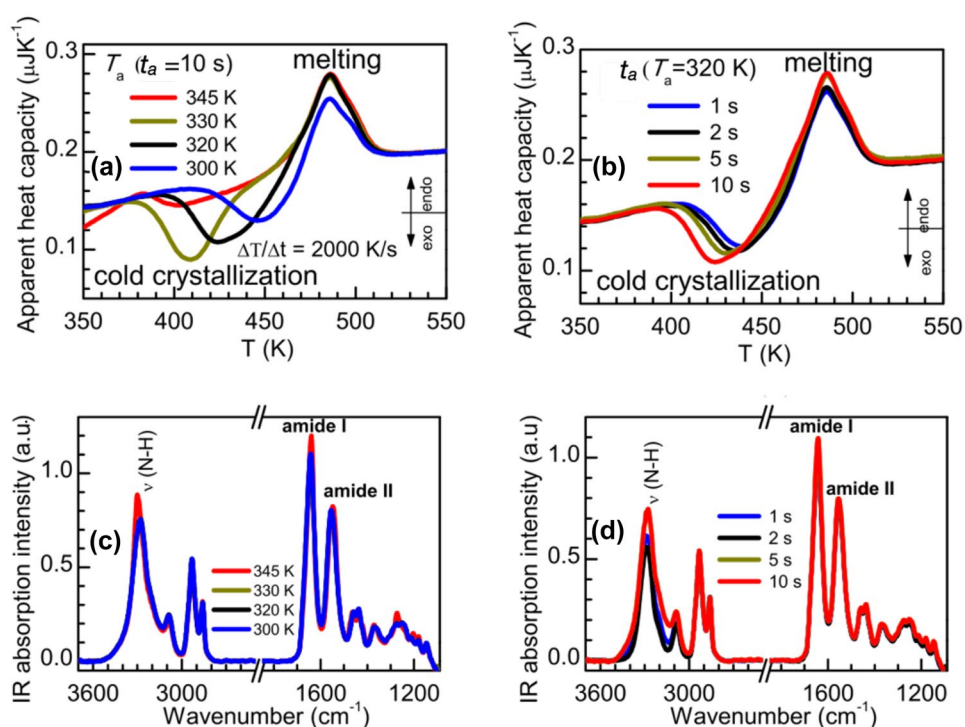
in Fig. 4 for the nucleation (Fig. 4a–c) and crystal growth regimes (Fig. 4d–f). During the initial stages of nucleation, the strength of the difference absorption spectra of $\nu(C=O)_b$ and $\nu(C=O)_f$ moieties (Fig. 4a) increase and decrease, respectively with increasing T_a. This trend is reversed for higher T_a (315–330 K). It implies a two-stage nucleation process prior to the onset of crystal growth.

In the crystal growth phase (Fig. 4d), the strength of IR absorption for $\nu(C=O)_b$ units again increases while that of $\nu(C=O)_f$ decreases. For comparison, the spectra obtained during the nucleation regime are also included in Fig. 4d. We attribute the changes observed during crystal growth to the increase in the H-bond bridges between the polymer segments as the sample attains a more ordered crystalline structure. This is also corroborated by a significant red shift of the amide II band by about 30 cm^{-1} in the crystal growth regime. Notably, other IR spectral regions, for instance the methylene $\delta(CH_2)$ scissoring vibrations and amide III bands, which are mainly due to the in-phase combination of $\delta(N-H)$ in-plane bending and $\nu(C-N)$ stretching vibrations [43] show changes only in the crystal growth but not during nucleation process (Fig. 4b, c, e, f). This is because nucleation is initiated by localized H-bond formation within the amorphous phase hence the non-polar moieties and IR vibrational modes with inference to the ordered sample geometry show insignificant spectral changes during nucleation.

In order to obtain quantitative data about the nucleation and subsequent crystallization as a function of T_a for different t_a, the enthalpy of cold-crystallization $\Delta h_{cold\ cryst.}$ and

the total enthalpy-change $\Delta h_{overall}$, from the FSC scans, were analysed. The cold-crystallization enthalpy was estimated by the integration of the corresponding exothermic cold-crystallization peaks using the heat capacity of liquid PA66 as baseline [44]. The total enthalpy change was obtained as the sum of the integral areas of the cold-crystallization and melting peaks after subtracting the integral value of the fully quenched sample. Within this framework, pure nucleation is denoted by an increase in the enthalpy of $\Delta h_{cold\ cryst.}$ while $\Delta h_{overall}$ remains at zero. Note that the negative values of $\Delta h_{cold\ cryst.}$ simply means that the process is exothermic. Crystal growth sets in when overall enthalpy $\Delta h_{overall}$ starts to increase from zero. Since we performed FTIR measurements on the same sample under similar conditions as FSC measurements, the above information becomes very important as it allows us to unequivocally distinguish the changes recorded by FTIR with respect to the thermodynamic state of the sample, i.e. nucleation or crystal growth regimes.

In order to gain more insight into the nucleation process in PA66, we plotted the $\Delta h_{cold\ cryst.}$ and $\Delta h_{overall}$ as a function of T_a for different t_a and compared with the maxima of the IR absorption peaks (obtained from difference spectra) for H-bonded and free $C=O$ moieties (Fig. 5a–p). For $T_a < 330$ K, the $\Delta h_{overall}$ remains at zero within experimental uncertainty. This implies that within this T_a regime, there is no crystal growth when $t_a < 10$ s, hence the changes exemplified by the IR data are solely due to the nucleation. The magnitude of $\Delta h_{cold\ cryst.}$ corresponds to the number or size of the nuclei formed [45]. Figure 5 shows that
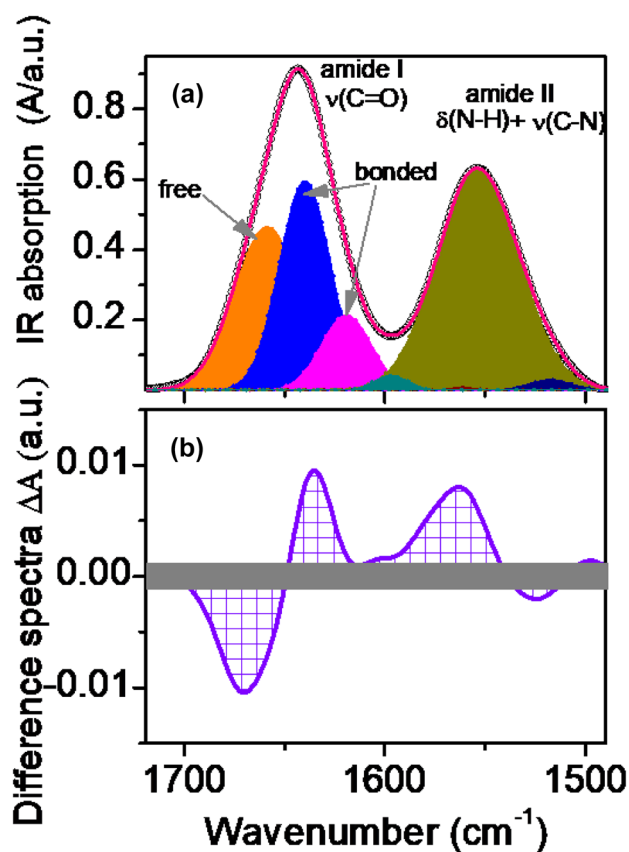
Fig. 3 **a** FTIR spectra of PA66 within amide I and II regions obtained at $T_a = 315$ K and $t_a = 5$ s. The line is the sum of the Gaussian fit functions to the data. The coloured regions represent individual convoluted peaks. Amide I region depicts three peaks assigned to free C=O moieties (extreme left) and H-bonded ones shown by the two peaks to the right. **b** The difference spectra between fully quenched sample and the sample annealed at $T_a = 315$ K and $t_a = 5$ s. The uncertainties in the difference absorption spectra are represented by the horizontal shaded strip

$\Delta h_{cold\ cryst.}$ remains relatively unchanged if $t_a < 10$ s, and T_a is between 300 and 315 K. On the contrary, we observe changes in IR data already within this T_a range whereby the IR absorption of H-bonded C=O moieties increases whereas that of free C=O decreases. This is attributed to the formation of H-bond bridges facilitated by the dipole–dipole interactions within the amorphous phase.

This densification process eventually leads to local ordering within initial nuclei. This is accompanied by a decrease in H-bonded and increase in free C=O moieties (Fig. 5b-h) implying that the sample changes to a structure that has reduced H-bond propensity. This is possible when the PA66 chains are aligned parallel to each other with untwisted conformation hence decreasing H-bond possibilities between C=O.

This is reminiscent to the γ polymorph mostly observed in PA6 [29]. In a combined FSC and X-ray nucleation and crystallisation study of PA66, Gohn et al. [9] identified less stable pseudohexagonal γ structures in PA66 at lower annealing temperatures. Recent X-ray studies also propose the existence of parallel pleated structures in crystalline PA66 with histories that involve self-seeding [30, 31]. Based on this information, we attribute the observed decrease of H-bonded C=O moieties to the formation of ordered domains consisting of unstable pleated parallel structures which we denote as γ polymorph. The pleated parallel chain orientation in this phase therefore results to an increase in the number of free C=O units.

Considering the data obtained from nanocalorimetry, the γ polymorph is formed within the nucleation regime. Consequently, we propose the structure of this γ phase as shown in Fig. 6. In this case, the H-bond formation between amide groups of neighbouring chains of PA66 is possible. This implies that during nucleation, N–H groups participate in two types of H-bonding, i.e. NH–O=C and NH–NH leading to the formation of γ polymorph which changes to α polymorph in the crystal growth regime. This is corroborated by the fact that the amide II band at around 1563 cm^{-1} decreases and disappears before a new amide II band at around 1535 appears and grows during crystallization as shown in Fig. 4d. The HN process in this sample therefore proceeds in two-stages. The first step involves the formation of two species of H-bonding network together with dipole–dipole interactions which increase within the disordered domains before the ordered γ phase is formed in the second stage. It is important to note that chain conformational/structural changes precede the dissociation of H-bonds [46] hence a dynamic equilibrium between H-bonds within amorphous and ordered domains exist.

According to the thermal preconditioning of the sample employed in this study, it is expected that the sample would exhibit an altered structural state for different t_a. In Fig. 5a–h, we note that the maximum for the intensity of the bonded C=O moieties is higher for shorter t_a and crystal growth start at higher T_a. Comparison of the FSC and IR data for the crystal growth regime is shown in Fig. 5i–p. As explained earlier, crystal growth sets in at the upturn of the $\Delta h_{overall}$. The transition between nucleation and crystallisation occurs over a wider temperature range for shorter t_a. During this time, the enthalpy changes and the IR absorption remains constant before $\Delta h_{cold\ cryst.}$ and $\Delta h_{overall}$ start to decrease and increase, respectively. The change of the slope corresponds to a shift to secondary crystallisation. Similarly, the change of the strength of IR absorption of H-bonded and free C=O groups increase and decrease, respectively. This is due to increased H-bond network in the crystalline structure. The common crystalline structure of PA66 is the triclinic α polymorph which consist of anti-parallel chains as sketched in Fig. 6.
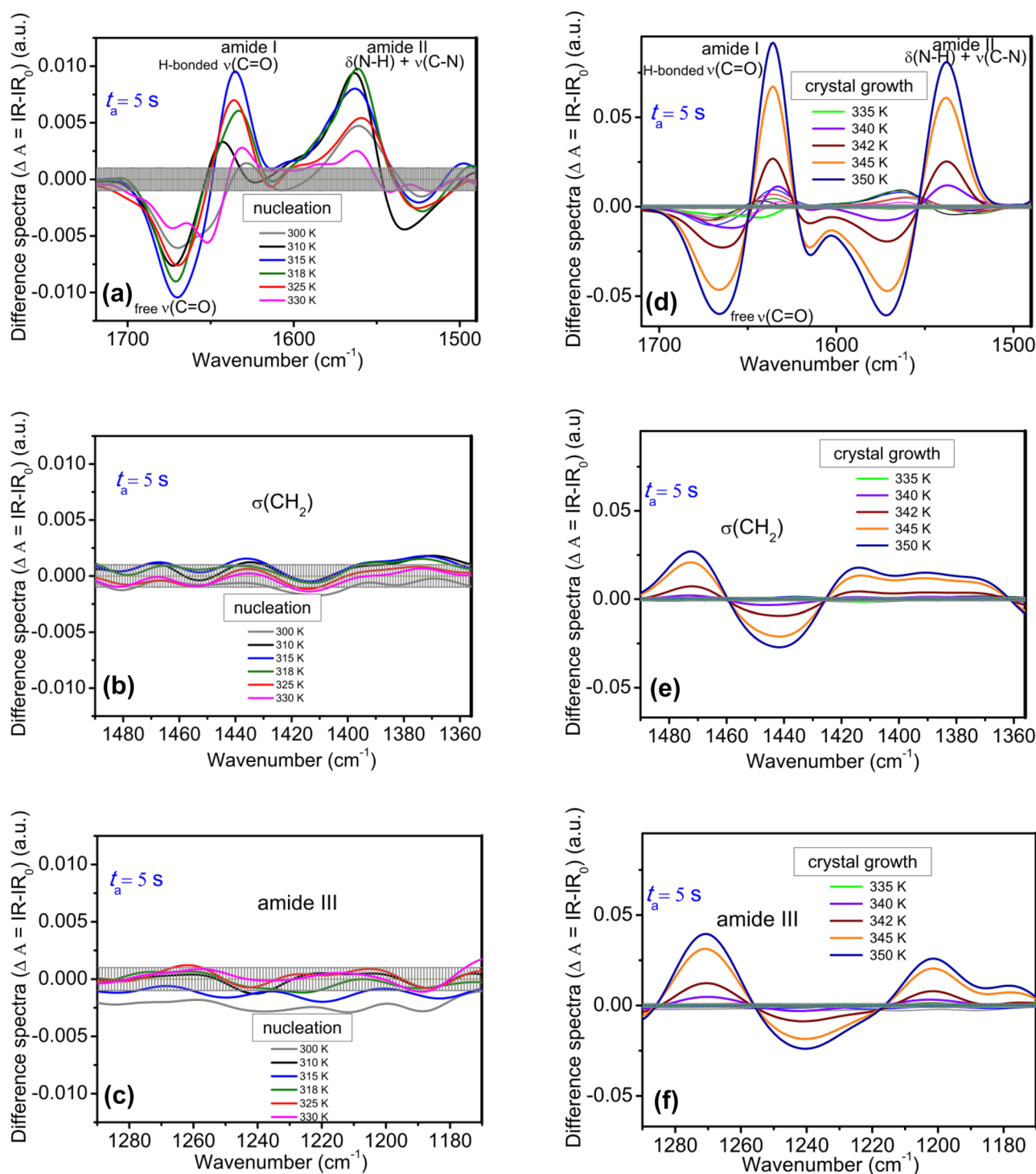
Fig. 4 IR difference spectra of PA66 between fully quenched state and when annealed for $t_a = 5$ s at the indicated temperatures T_a where nucleation (**a**–**c**) and crystal growth (**d**–**f**) take place. In the nucleation regime, changes larger than the noise level (grey shaded regions) are only observed for the amide I and II bands; in contrast for crystal growth, pronounced differences are manifested for the amide I, II, and III and the methylene scissoring vibrations $\sigma(CH_2)$. Watch the varying scales in the difference spectra. The low intensity peaks in **d** represent the nucleation regime as shown in **a**
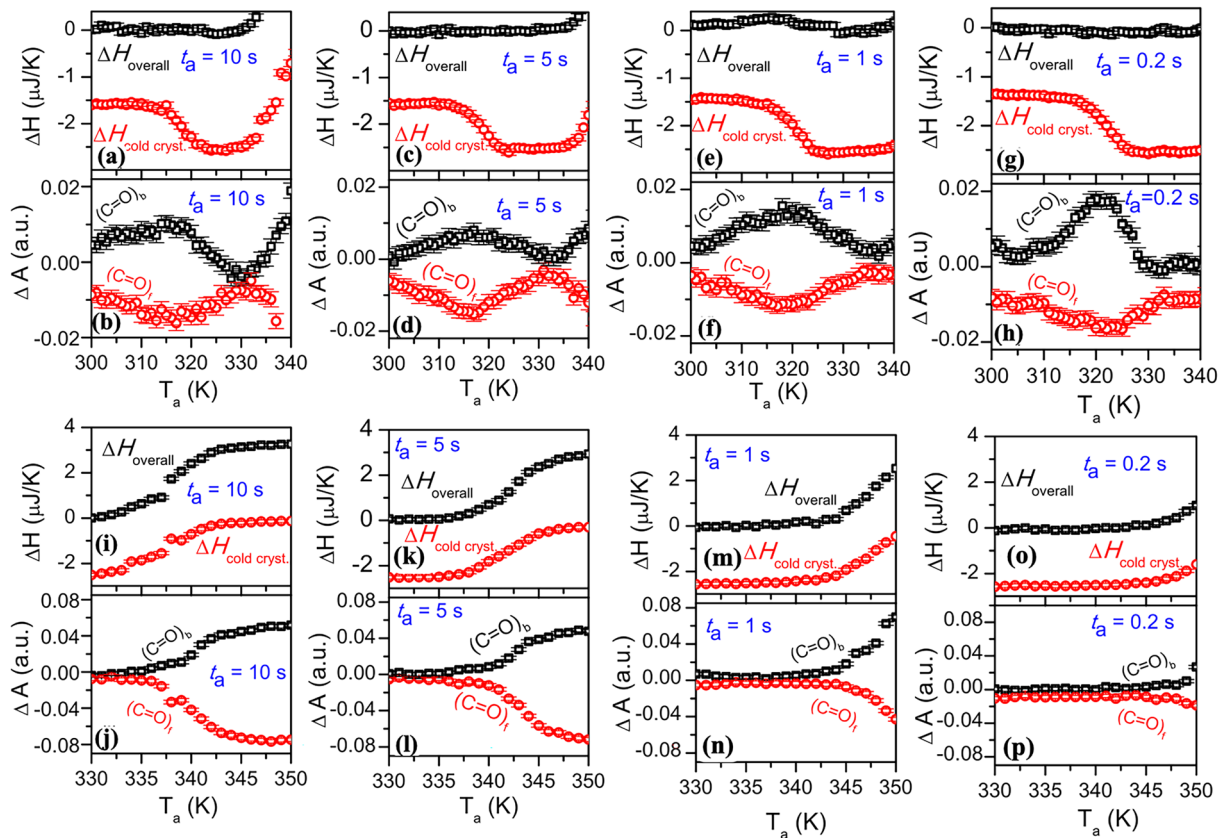
Fig. 5 The FSC data depicting the overall enthalpy changes (black symbols) and the enthalpy of cold crystallisation (red symbols) as a function of T_a for $t_a = 10$, 5, 1, and 0.2 s are shown in **a**, **c**, **e**, and **g**, respectively. The overall enthalpy change is determined from the sum of the areas under positive melting and the negative cold crystallization enthalpies (shown in Fig. 2a, b). Crystallization starts when the overall enthalpy changes deviate from zero or equivalent to the minimum of the cold crystallization enthalpy. **b**, **d**, **f**, and **h** are the corresponding FTIR data showing the absorption intensities of H-bonded (black symbols) and free (red symbols) C=O moieties as obtained from the difference spectra. The corresponding data for the crystal growth regime are shown in **i–p**

Fig. 6 Schematic representation of the evolution of the PA66 sample from the quenched state through nucleation to crystalline state. The scale bar shown in the top sketches represents an approximated length scale
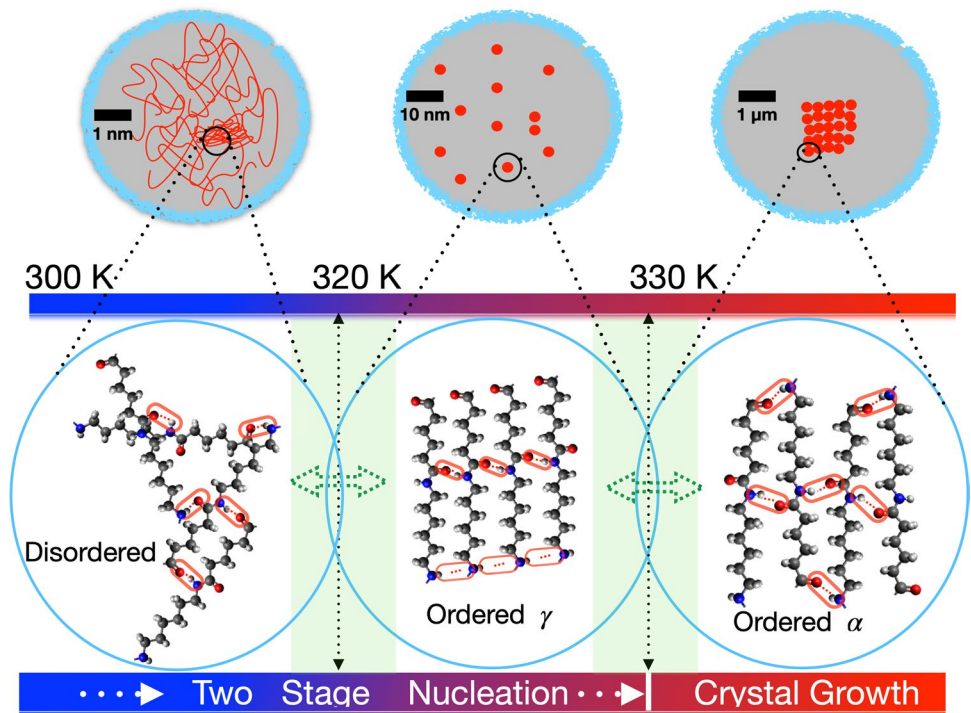
Conclusions

In summary, molecular mechanisms leading to the homogeneous nucleation in polyamide 66 sample have been studied by in situ nanocalorimetry and FITR spectroscopy on the *identical* sample. This approach allows to quench the sample at ultrafast rates from the molten state to the desired temperature while avoiding crystallisation and homogeneous nucleation. FTIR characterizations and the thermodynamics of phase transformation were performed as functions of isothermal annealing temperature and time. By analysing the IR difference spectra of amide I and II bands depending on the annealing temperature (T_a) at constant annealing time (t_a), we show that within the nucleation regime ($T_a < 330$ K), the H-bonded C=O moieties increase and then decrease before a monotonous increase again at higher T_a. This is attributed to the existence of a two-stage nucleation mechanism involving formation of higher density regions within the amorphous phase where metastable structures/polymorphs develop and already transform to more stable crystalline structures at elevated T_a within the given t_a. This approach opens up the opportunity for similar studies that may unravel underlying nucleation mechanism for instance in the formation of amyloids in proteins, or the liquid–liquid transitions.

Declarations

Conflict of interest The authors declare no competing interests.

References

1. La Carrubba V, Brucato V, Piccarolo S (2002) Influence of "controlled processing conditions" on the solidification of iPP, PET and PA6. Macromol Symp 180:43–60. https://doi.org/10.1002/1521-3900(200203)180:1%3c43::AID-MASY43%3e3.0.CO;2-Z

2. Rhoades AM, Williams JL, Androsch R (2015) Crystallization kinetics of polyamide 66 at processing-relevant cooling conditions and high supercooling. Thermochim Acta 603:103–109. https://doi.org/10.1016/j.tca.2014.10.020

3. Anton AM, Zhuravlev E, Kossack W et al (2020) Fingerprints of homogeneous nucleation and crystal growth in polyamide 66 as studied by combined infrared spectroscopy and fast scanning chip calorimetry. Colloid Polym Sci 298:697–706. https://doi.org/10.1007/s00396-020-04666-9

4. Sangroniz L, Cavallo D, Müller AJ (2020) Self-nucleation effects on polymer crystallization. Macromolecules 53:4581–4604. https://doi.org/10.1021/acs.macromol.0c00223

5. Androsch R, Schick C (2017) Crystal nucleation of polymers at high supercooling of the melt. In: Auriemma F, Alfonso GC, de Rosa C (eds) Polymer crystallization I: from chain microstructure to processing. Springer International Publishing, Cham, pp 257–288

6. Thomas D, Schick C, Cebe P (2018) Novel method for fast scanning calorimetry of electrospun fibers. Thermochim Acta 667:65–72. https://doi.org/10.1016/j.tca.2018.07.001

7. Michell RM, Blaszczyk-Lezak I, Mijangos C, Müller AJ (2013) Confinement effects on polymer crystallization: from droplets to alumina nanopores. Polymer 54:4059–4077. https://doi.org/10.1016/j.polymer.2013.05.029

8. Gao Y, Zhao B, Vlassak JJ, Schick C (2019) Nanocalorimetry: door opened for in situ material characterization under extreme non-equilibrium conditions. Prog Mater Sci 104:53–137. https://doi.org/10.1016/j.pmatsci.2019.04.001

9. Gohn AM, Rhoades AM, Wonderling N et al (2017) The effect of supercooling of the melt on the semicrystalline morphology of PA 66. Thermochim Acta 655:313–318. https://doi.org/10.1016/j.tca.2017.07.012

10. Androsch R, Iqbal HMN, Schick C (2015) Non-isothermal crystal nucleation of poly (l-lactic acid). Polymer 81:151–158. https://doi.org/10.1016/j.polymer.2015.11.006

11. Androsch R, Di Lorenzo ML, Schick C (2018) Optical microscopy to study crystal nucleation in polymers using a fast scanning chip calorimeter for precise control of the nucleation pathway. Macromol Chem Phys 219:1700479. https://doi.org/10.1002/macp.201700479

12. Zhang R, Zhuravlev E, Schmelzer JWP et al (2020) Steady-state crystal nucleation rate of polyamide 66 by combining atomic force microscopy and fast-scanning chip calorimetry. Macromolecules 53:5560–5571. https://doi.org/10.1021/acs.macromol.0c00574

13. Wei L, Jiang J, Shan M et al (2014) Integration of ultrafast scanning calorimetry with micro-Raman spectroscopy for investigation of metastable materials. Rev Sci Instrum 85:074901. https://doi.org/10.1063/1.4889882

14. Skrovanek DJ, Howe SE, Painter PC, Coleman MM (1985) Hydrogen bonding in polymers: infrared temperature studies of an amorphous polyamide. Macromolecules 18:1676–1683. https://doi.org/10.1021/ma00151a006

15. Cooper SJ, Coogan M, Everall N, Priestnall I (2001) A polarised μ-FTIR study on a model system for nylon 6 6: implications for the nylon Brill structure. Polymer 42:10119–10132. https://doi.org/10.1016/S0032-3861(01)00566-3

16. Li Y, Yan D, Zhou E (2002) In situ Fourier transform IR spectroscopy and variable-temperature wide-angle X-ray diffraction studies on the crystalline transformation of melt-crystallized nylon 12 12. Colloid Polym Sci 280:124–129. https://doi.org/10.1007/s003960100571

17. Rotter G, Ishida H (1992) FTIR separation of nylon-6 chain conformations: Clarification of the mesomorphous and γ-crystalline phases. J Polym Sci Part B Polym Phys 30:489–495. https://doi.org/10.1002/polb.1992.090300508

18. Ma Y, Zhou T, Su G et al (2016) Understanding the crystallization behavior of polyamide 6/polyamide 66 alloys from the perspective of hydrogen bonds: projection moving-window 2D correlation FTIR spectroscopy and the enthalpy. RSC Adv 6:87405–87415. https://doi.org/10.1039/C6RA09611E

19. Yang T, Gao Y, Wang X et al (2021) Hydrogen bonding and crystalline structure of bio-based PA56. Polymer 237:124356. https://doi.org/10.1016/j.polymer.2021.124356

20. Zhang X, Gohn A, Mendis G et al (2021) Probing three distinct crystal polymorphs of melt-crystallized polyamide 6 by an integrated fast scanning calorimetry chip system. Macromolecules 54:7512–7528. https://doi.org/10.1021/acs.macromol.1c00811

21. Li X, He Y, Dong X et al (2020) Effects of hydrogen-bonding density on polyamide crystallization kinetics. Polymer 189:122165. https://doi.org/10.1016/j.polymer.2020.122165

22. Joseph J, Jemmis ED (2007) Red-, blue-, or no-shift in hydrogen bonds: a unified explanation. J Am Chem Soc 129:4620–4632. https://doi.org/10.1021/ja067545z

23. Rozenberg M, Shoham G, Reva I, Fausto R (2005) A correlation between the proton stretching vibration red shift and the hydrogen bond length in polycrystalline amino acids and peptides. Phys Chem Chem Phys 7:2376–2383. https://doi.org/10.1039/B503644E

24. Rozenberg M, Loewenschuss A, Marcus Y (2000) An empirical correlation between stretching vibration redshift and hydrogen bond length. Phys Chem Chem Phys 2:2699–2702. https://doi.org/10.1039/B002216K

25. Gabriel JP, Tress M, Kossack W et al (2021) Molecular heterogeneities in the thermal expansivity of polyalcohols. J Chem Phys 154:024503. https://doi.org/10.1063/5.0036067

26. Hydrogen bonding and dynamic crossover in polyamide-66: a molecular dynamics simulation study. Macromolecules 2008, 41, 19, 7211–7218. https://doi.org/10.1021/ma8010685

27. Murthy NS (2006) Hydrogen bonding, mobility, and structural transitions in aliphatic polyamides. J Polym Sci Part B Polym Phys 44:1763–1782. https://doi.org/10.1002/polb.20833

28. Coussens B, Rulkens R (2018) Effect of amide distribution in polyamide isomers on their melting points. J Appl Polym Sci 135:45837. https://doi.org/10.1002/app.45837

29. Seguela R (2020) Overview and critical survey of polyamide6 structural habits: misconceptions and controversies. J Polym Sci 58:2971–3003. https://doi.org/10.1002/pol.20200454

30. Lotz B (2021) Original crystal structures of even–even polyamides made of pleated and rippled sheets. Macromolecules 54:551–564. https://doi.org/10.1021/acs.macromol.0c02404

31. Lotz B (2021) A fresh look at the structures of nylons and the brill transition. Adv Fiber Mater 3:203–209. https://doi.org/10.1007/s42765-021-00085-9

32. Puiggalí J (2021) Aliphatic polyamides (nylons): Interplay between hydrogen bonds and crystalline structures, polymorphic transitions and crystallization. Polym Cryst 4:e10199. https://doi.org/10.1002/pcr2.10199

33. Vekilov PG (2010) Nucleation. Cryst Growth Des 10:5007–5019. https://doi.org/10.1021/cg1011633

34. Zhang TH, Liu XY (2009) Nucleation: what happens at the initial stage? Angew Chem 121:1334–1338. https://doi.org/10.1002/ange.200804743

35. Selective nucleation and discovery of organic polymorphs through epitaxy with single crystal substrates. J Am Chem Soc 2001, 123, 44, 10830–10839. https://doi.org/10.1021/ja004085f

36. Towler CS, Davey RJ, Lancaster RW, Price CJ (2004) Impact of molecular speciation on crystal nucleation in polymorphic systems: the conundrum of γ glycine and molecular 'self poisoning.' J Am Chem Soc 126:13347–13353. https://doi.org/10.1021/ja047507k

37. Wu K-J, Tse ECM, Shang C, Guo Z (2022) Nucleation and growth in solution synthesis of nanostructures – from fundamentals to advanced applications. Prog Mater Sci 123:100821. https://doi.org/10.1016/j.pmatsci.2021.100821

38. Erdemir D, Lee AY, Myerson AS (2009) Nucleation of crystals from solution: classical and two-step models. Acc Chem Res 42:621–629. https://doi.org/10.1021/ar800217x

39. Tang X, Yang J, Xu T et al (2017) Local structure order assisted two-step crystal nucleation in polyethylene. Phys Rev Mater 1:073401. https://doi.org/10.1103/PhysRevMaterials.1.073401

40. Taylor AIP, Gahan LD, Chakrabarti B, Staniforth RA (2020) A two-step biopolymer nucleation model shows a nonequilibrium critical point. J Chem Phys 153:025102. https://doi.org/10.1063/5.0009394

41. Lutsko JF (2019) How crystals form: a theory of nucleation pathways. Sci Adv 5(4):1–8. https://doi.org/10.1126/sciadv.aav7399

42. Ultra-strong long-chain polyamide elastomers with programmable supramolecular interactions and oriented crystalline microstructures. Nat Commun 10:1315. https://www.nature.com/articles/s41467-019-09218-6

43. Cai S, Singh BR (2004) A distinct utility of the amide III infrared band for secondary structure estimation of aqueous protein solutions using partial least squares methods. Biochemistry 43:2541–2549. https://doi.org/10.1021/bi030149y

44. Steady-state crystal nucleation rate of polyamide 66 by combining atomic force microscopy and fast-scanning chip calorimetry. Macromolecules 2020, 53, 13, 5560–5571. https://doi.org/10.1021/acs.macromol.0c00574

45. Zhuravlev E, Schmelzer JWP, Wunderlich B, Schick C (2011) Kinetics of nucleation and crystallization in poly(ε-caprolactone) (PCL). Polymer 52:1983–1997. https://doi.org/10.1016/j.polymer.2011.03.013

46. Wu P, Siesler HW (2000) Two-dimensional correlation analysis of variable-temperature Fourier-transform mid- and near-infrared spectra of polyamide 11☆In honour of Professor Giuseppe Zerbi on the occasion of his 65th birthday.☆. J Mol Struct 521(1–3):37–47. https://doi.org/10.1016/S0022-2860(99)00424-X

Springer